Supplementary Materials for

Structure and Organization of Heteromeric AMPA-type Glutamate Receptors

Beatriz Herguedas, Javier García-Nafría, Ondrej Cais, Rafael Fernández-Leiro, James Krieger, Hinze Ho, Ingo H. Greger

correspondence to: ig@ mrc-lmb.cam.ac.uk

This PDF file includes:

Other Supplementary Materials for this manuscript include the following:

Materials and Methods

Cloning, expression and protein purification

The plasmids used for full-length receptors were: 1) the rat *GRIA2* cDNA (flip splice variant, fully edited at the R/G and Q/R editing sites) containing a N-terminal c-myc tag or a N-terminal FLAG tag in the pIRES2-EGFP vector, 2) the rat *GRIA3* cDNA (flip, R439G) with a N-terminal FLAG tag in the pRK5 vector (for protein production and biochemical assays) and in the pIRES2-mCherry vector (for electrophysiological studies) and 3) the rat GluA4 cDNA (flip) with and without an N-terminal FLAG-tag in the pRK5 vector. All site-directed mutagenesis was performed on these constructs including the GluA2myc N292C, V209C and N292C+V209C, GluA3flag R265C and GluA4flag R264C, and GluA4 S172C and Q175C.

For crystallization, GluA2 NTD (residues 1-379 of the mature protein), GluA3 NTD (1-380 of the mature protein) and GluA4 NTD (1-380 of the mature protein) were produced in stably transfected HEK293S-GnTI$^-$ cells as previously described (*18*). Briefly, purification consisted of cross-flow concentration and dialysis (in 1 M NaCl, 50 mM Tris pH 8) followed by affinity (His-trap HP column, GE Healthcare) and size exclusion chromatography (S200, GE Healthcare). Oligosaccharides were removed from the protein sample using enzymatic EndoH treatment in 100 mM sodium acetate pH 5.2 and further purification by size exclusion chromatography in 50 mM HEPES pH 7.4, 150 mM NaCl.

For the purification of the full-length cross-linked receptor, GluA2myc N292C (flip, R/G, Q/R) and GluA3flag R265C (flip, R439G) plasmids were transfected into HEK293S-GnTI$^-$ cells (*38*) grown in suspension. Cell culture and transfection were performed following recently described protocols (*39, 40*). For 1 l of cells (3 x 10^6 cells/ml), a transfection mixture was prepared containing 0.8 mg of GluA2 plasmid, 0.2 mg of GluA3 plasmid and 3 ml of PEI-max (Polysciences inc) at 1 mg/ml in 80 ml of Hybridoma medium (Life Technologies). Prior to transfection, cells were centrifuged at 400 g and supernatant removed. Cells were resuspended in the transfection mixture and added to 670 ml of Freestyle medium supplemented with 1% FBS. Cells were grown at 37 °C for 60 hours and harvested by centrifugation. Cell pellets were resuspended in ice-cold PBS containing 10 μM copper phenanthroline (mixed from $CuCl_2$ and 1,10-phenanthroline at a 1:3 molar ratio; values in the text representing the $CuCl_2$ concentration) and harvested by centrifugation at 800 g. Cells were lysed for 90 minutes at 4 °C in 25 mM Tris pH 7.4, 150 mM NaCl, 1% *n*-dodecyl-β-D-maltoside (DDM), 1x Protease Inhibitors Cocktail (Roche), 30 mM N-ethylmaleimide (NEM), 1 mM phenylmethanesulfonyl fluoride (PMSF). After centrifugation, the supernatant was incubated with anti-FLAG M2 beads (Sigma) for 2 h at 4 °C. Sample was eluted with buffer containing 0.15 mg/ml FLAG peptide (Sigma), 0.25% DDM, 25 mM Tris pH 7.4, 150 mM NaCl. To isolate the heteromeric pool of receptors, a second affinity purification was performed, incubating with anti-myc affinity beads (Pierce). Sample was eluted with 0.5 mg/ml c-myc peptide (Pierce), 0.25 % DDM, 25 mM Tris pH 7.4, 150 mM NaCl. The eluted sample at 0.03 mg/ml showed two bands in non-reducing SDS-PAGE corresponding to monomers and disulfide-linked dimers (fig. S4A).

Crystallization, data collection and structure determination of NTD heteromers

For GluA2/3 crystallization, GluA3 NTD was diluted to 5 mg/ml and GluA2 NTD (0.5 mg/ml) was added and concentrated in sequential steps until the GluA2/3 molar ratio reached 1:1 achieving a final concentration of 22 mg/ml. For GluA2/4 heteromers, both GluA2 and GluA4 NTDs were diluted to 0.5 mg/ml, mixed at 1:1 molar ratio and concentrated to 14 mg/ml. Crystallization screens were set in 96-well MRC plates in 150 nl + 150 nl drops, with the protein at 12.5 mg/ml. GluA2/3 crystals appeared in drops containing 14-16 % PEG 3350, 0.27 M ammonium sulphate and 0.1 M Bicine pH 9. GluA2/4 crystals grew in 17% PEG 3350 with 0.1-0.35 M ammonium sulphate. Crystals were cryoprotected with 20 % glycerol and flash-frozen in liquid nitrogen. Data collection was performed in Diamond Light Source at the I04-1 beamline (0.9163 Å wavelength) and data were collected to 2.12 (GluA2/3) and 2.5 Å resolution (GluA2/4). GluA2/3 data were integrated, scaled and reduced with *Xia2* (*41*). GluA2/4 data were integrated with iMosflm (*42*) and scaled and reduced with AIMLESS (*43*). The GluA2/3 structure was determined by molecular replacement using monomers from 3HSY (GluA2) (*18*) and 3O21 (GluA3) (*19*) as search models in MOLREP (*44*). 3HSY (GluA2) and 4GPA (GluA4) (*45*) were used as search models to phase the GluA2/4 structure by molecular replacement using PHASER (*46*). Both structures were refined using REFMAC5 (*47*) from the CCP4 suite of programs (*48*) and manual modifications were performed with COOT (*49*). The structures were refined to R_{work}/R_{free} of 19.2/23.1 % and 17.4/23.8 % for GluA2/3 and GluA2/4, respectively, both presenting good geometry as defined by the Ramachandran plot. TLS and individual isotropic B factors were refined in both structures. The GluA2/4 structure presented pseudo-symmetry (as shown by the Patterson map) and pseudo-merohedral twinning with a monoclinic cell with a β angle close to 90°. To overcome this problem, refinement was carried out computing the twinning fraction using REFMAC5 (twinning fraction of 0.5).

Disulphide crosslinking experiments of full-length heteromers

Mutants were transfected into HEK293T cells using the Effectene® transfection reagent (Qiagen) using a 1:4 ratio of the GluA3-pRK5:GluA2-pIRES2-EGFP plasmids. Following expression for ~ 60 hours, cells were treated with ice-cold PBS containing 10 μM copper phenanthroline (as above) for 45 min prior to harvesting and lysing in 25mM HEPES pH 7.5, 150 mM NaCl, 1 mM EDTA, 1% Triton X-100, 50 mM NEM, together with PMSF and protease inhibitors cocktail (Roche). The lysate was incubated overnight with anti-FLAG® M2 magnetic beads, washed three times with lysis buffer and protein eluted with 2x SDS-PAGE loading dye. After 10 min incubation at 70 °C, samples were loaded into 3-8% Tris Acetate polyacrylamide gels, transferred into nitrocellulose membranes and probed with the Millipore anti-GluA2 AB1768 and anti-GluA4 AB1508. The anti-rat light chain MAB-201P secondary antibody was used. Signal was achieved using Supersignal® WestDura (Thermo Scientific) and images were recorded in a ChemiDoc MP system (BioRad). For native gels, cells were lysed in 1 % DDM instead of Triton X-100. Lysate was incubated with anti-FLAG® M2 magnetic beads, washed 3 times and eluted with 6 volumes of 0.1 mg/ml Flag peptide in NativePage™ sample buffer supplemented with 1 % DDM. Samples were loaded into NativePAGE™ Novex® 4-16% Bis-Tris gels, and run following the manufacturer protocol. Samples were

transferred to PVDF membranes prior to blocking with 5% milk and probed with Anti-GluR2 C-terminal antibody (Sigma). Signal development was carried out as described before. Controls including SDS and SDS+DTT were also included in the gel.

Electron microscopy sample preparation and data acquisition

For negative staining, aliquots of 4 µL sample at ~ 0.03 mg/ml were stained using 0.75 % (w/v) uranyl formate on glow discharged 400 mesh copper grids (Agar Scientific) covered with a thin layer of carbon. When appropriate, samples were mixed with 100 mM glutamate immediately before grid preparation, or incubated with 10 mM DTT for 1 h at 4 °C prior to adding 100 mM glutamate. Images were recorded using a Tecnai T12 electron microscope (FEI company) operated at 120 kV with a nominal magnification of 30,000x (pixel size 3.286 Å) for the crosslinked apo and glutamate samples and at 26,000x (pixel size 3.84 Å) for the glutamate + DTT samples. All data were collected at ~ 1 µm defocus using 1-second exposures, 20 electron per $Å^2$ per s using a Gatan Ultrascan 1000 2Kx2K with a 14µm pixel size.

For cryo-EM, R1.2/1.3 Quantifoil 300 mesh copper grids covered with a thin layer of carbon were rendered hydrophilic using glow discharge. Vitrified specimens were prepared using an FEI Vitrobot MKIII at 100 % humidity and 4 °C, where 4 µL samples at 0.03 mg/ml were incubated for 1 minute, blotted for 3 seconds and plunge-frozen in liquid ethane. Images were recorded on an FEI Titan Krios microscope (FEI Company) operated at 300 kV using a K2 Summit detector in single-electron counting mode, resulting in a calibrated magnification of 28,409x (1.76 Å/pixel). The K2 Summit detector was mounted after a Gatan Imaging Filter (GIF-Quantum energy filter) and a slit width of 20 eV was used to remove inelastic scattered electrons. A dose rate of 1.6 electrons per $Å^2$ per s and a total exposure of 40 electrons per $Å^2$ were used, with a total of 20 movie frames recorded. Defocus values ranged from 1 to 4 µm.

Image processing and model building

For the analysis of images from negatively stained samples EMAN2 (*50*) was used for initial manual and semi-automated particle picking and RELION (*30*) was used for all subsequent steps. Initial 2D representative classes were used for automated selection of particles in RELION. Four to six rounds of false positive elimination by reference-free two-dimensional classification rendered 34,836 particles for the $GluA2/3_{xlink}$, 27,648 particles for the glutamate-treated sample and 36,966 particles for the glutamate + DTT-treated sample. For the three-dimensional classification two different initial models were used. First, an O-shape model was built using the transmembrane and ligand binding domain of the $GluA2_{cryst}$ (PDB code 3KG2) and our tetrameric crystal structure of the GluA2/3 NTDs. A second model, with an N-shape NTD, was generated using the whole GluA2 homomer structure (PBD code 3KG2). Both models were low-pass filtered to 60 Å. Using these as starting references for 3D classification in the $GluA2/3_{xlink}$ dataset, we obtained classes with O-like arrangements at the NTD layer. For the remaining datasets the O-model was used as the starting model for 3D classification. All datasets were divided into five classes and the cleanest model was chosen for refinement. Both $GluA2/3_{xlink}$ and $GluA2/3_{xlink}$ + Glu samples yielded maps at ~ 20 Å resolution with

models containing 9211 particles for the GluA2/3$_{xlink}$ and 6684 particles for the glutamate-treated sample. To further validate the model, an NTD-lacking map, filtered at 60 Å was generated and used as the initial model for the refinement. Here the resulting map showed an O-shape structure appearing unambiguously after refinement. A population of Y-shape receptors also appeared in the 3D classification but the amount varied randomly with the sample preparation.

For cryo-EM, movie frames for each micrograph were aligned for whole-image drift using MOTIONCORR (*51*) and contrast transfer function parameters were estimated with Gctf (*52*). EMAN2 was used for initial manual and semi-automated particle picking and RELION was used for 2D classification as well as subsequent classification and refinement unless otherwise stated. Resulting 2D classes were fed as references for automated picking with RELION. Particles were extracted in a 288 Å box for reference-free two-dimensional classification, which rendered 107,939 particles to be used for subsequent three-dimensional analysis. In order to produce a starting reference free of bias, an *ab-initio* model was created starting with representative 2D classes in EMAN2. Beam-induced movement correction and B-factor weighting were performed by applying statistical movie processing in RELION (*30*). 3D classification resulted in three classes featuring O-like NTDs (73,885 particles) and one class resembling classical Y-shaped receptor (16,697 particles) (fig. S9). The fifth class contained particles forming an uninterpretable model and was therefore discarded. Further 3D-classification of the O-like classes using a soft mask allowed us to eliminate false positives and to obtain two improved classes with two clearly different conformations at the LBD layer (fig. S9). The soft-edge mask was created with relion_mask_create extending the map 5 pixels with a 5 pixels fall-off. The two classes were further classified in 3 classes to improve homogeneity, obtaining two maps that after refinement, produced the final maps M1 and M2 with overall resolutions of 8.25 and 10.3 Å respectively (fig. S10 and S11). Reported resolutions are calculated following the gold-standard FSC-0.143 criterion (*53*). Convolution effects on the FSC-curves were corrected using high-resolution noise substitution (*54*) (fig. S10). Maps were corrected for the modulation transfer function of the detector and sharpened by applying a negative B-factor. Xmipp (*55*) was used to calculate the FSC of the model *vs.* map. Local resolution analysis was performed with ResMap (*56*). A tilt-pair validation was performed in order to confirm the correctness of the map (fig. S10F).

Nine independent crystal structures of the different domains were rigid-body fitted into the M1 model using Chimera (*57*). The NTD layer was fitted using the GluA2 NTD (PDB code 3HSY, chain B) (*18*) and GluA3 NTD (PDB code 3O21, chain D) (*19*). For the TMD layer, coordinates of the antagonist-bound GluA2 homomer (PDB code 3KG2) (*5*) were used with removal of the re-entrant pore loop, for which density was absent. For the LBDs, over 100 crystal structures in complex with different ligands are currently available, displaying different levels of clamshell closure. We used the program NORMA (*58*) to assign the conformation of each LBD protomer in the EM-map. The ligand-free GluA2 LBD monomer (PDB code 1FTO) (*59*), placed in each of the four LBD positions in the EM map, was subjected to coordinate normal mode calculation coupled to a scoring system that assessed the fitness of each conformation to the EM map. For GluA2 the resulting conformation corresponded to the ligand-free state (PDB code 1FTO, chain B), and for GluA3 a conformation similar to GluA2 in complex with a

6-aminoquinazolinedione sulfonamide antagonist (PDB code 3UA8) (*60*), with an opening angle higher than any current GluA3 LBD structure and similar to the 1FTO opening angle. The same coordinates were used in the fitting of M2; however, the resolution of M2 did not allow for a calculation of LBD cleft angle. Final PDBs were created by renumbering and merging the fitted PDBs in PyMOL (*61*). Although the GluA2 and GluA3 C-termini were present, no density was observed in any of the cryo-EM maps, suggesting that these 50 amino acid segments are disordered.

Electrophysiology, data acquisition and analysis

HEK293T cells were co-transfected with GluA2 (flip) and GluA3 (flip, R439G) or GluA4 (flip) plasmids using the Effectene® transfection reagent (Qiagen) at ratios favoring the formation of heteromers (checked for each cell by recording the I/V characteristics of the responses in the presence of intracellular spermine).

Current responses of whole lifted cells, voltage-clamped at -60 mV, were elicited by fast application of 10 mM L-glutamate via a Θ-tube and recorded using an Axopatch-1D, -200B or -700B amplifier, a Digidata1322/1440A interface and pClamp 9.2/10.5 software (Molecular Devices). Cells were perfused with external solution containing (in mM): NaCl (145), KCl (3), $CaCl_2$ (2), $MgCl_2$ (1), glucose (10) and HEPES (10), adjusted to pH 7.4 with NaOH and supplemented with either 10 μM copper phenanthroline (CuPhe) or 10 mM dithiothreitol (DTT). Electrodes were fabricated from borosilicate glass (1.5mm o.d., 0.86mm i.d., Science Products GmbH) pulled with a PC-10 vertical puller (Narishige). When filled with the 'internal' solution, containing (mM): CsF (120), CsCl (10), EGTA (10), ATP-sodium salt (2), HEPES (10) and spermine (0.1), adjusted to pH 7.3 with CsOH, they had a final resistance of 2-5 MΩ. The oxidizing/reducing potency of the CuPhe/DTT solutions was checked routinely using the GluA2 S729C mutant (*62*).

To assess desensitization kinetics responses to 100 ms glutamate pulses were recorded and the current decay during the agonist application was fitted with a one- or two-exponential function to obtain the (weighted) time constant of desensitization ($\tau_{w,des}$). Recovery from desensitization was tested using a two-pulse protocol with a desensitizing 100 ms pulse followed by a 10 ms pulse in increasing intervals. The relative responses to the second pulse (an average of three consecutive runs) were plotted against time elapsed from the end of the first pulse and fitted by the Hodgkin-Huxley equation, as in (*63*).

The effect of forming/breaking the introduced Cys-bond was examined by recording each cell under both oxidizing and reducing conditions and comparing the parameters to the corresponding wild type (wt) receptors using repeated measures two-way ANOVA. This provides information about the effect of the mutation, the treatment (ox/red), and the interaction of the two factors, i.e. whether the effect of the treatment is different for the mutant and the wt.

Anisotropic Network Model (ANM) analysis

Normal mode analysis is a method for determining modes of motion accessible to a protein given a particular starting structure and a model describing forces between atoms.

The ANM is a coarse-grained elastic network model with a single node for each amino acid residue and interactions modeled as uniform harmonic springs between residues within a cut-off (15 Å between Cα atoms) (*26, 64*). The Hessian matrix of force constants (second derivative of the energy potential function) is decomposed to give a unique set of normal modes. Modes are represented by 3N-dimensional eigenvectors $\mathbf{u}_k$ (for N residues in 3D space) with corresponding eigenvalues λ_k. The first modes (those with low eigenvalues) describe low energy global motions and the higher modes describe less favourable local deformations. Conformations $\mathbf{R}^{(k)}$ along a given mode k were generated using the following equation $\mathbf{R}^{(k)} = \mathbf{R}^{(0)} \pm s\lambda^{-1/2}\mathbf{u}_k$ where $\mathbf{R}^{(0)}$ is a 3N-dimensional vector representing the initial coordinates and s is a scaling constant that can be adjusted to fit experimental data (*65*). Normal mode analysis (NMA) with the anisotropic network model (ANM) was carried out using the ANM Server (*66*) and Python extension ProDy (*67*) as previously described (*27*). Similarity between conformations along ANM mode 4 and the GluA2/3 NTD crystal structure was assessed using the Normal Mode Wizard (*67*) in VMD (*68*).

Comparing normal modes to transitions between N and O crystal structures

Transitions were calculated as the displacement vector for all corresponding Cα atoms required to interconvert the two aligned structures (N-shaped NTD layer from GluA2 homomer [PDB 3KG2] and our O-shaped GluA2/3 NTD crystal structure). The extent of directional overlap between a displacement vector $\mathbf{d}$ and a normal mode vector $\mathbf{u}_k$ generated from one of the aligned structures could then be calculated as the correlation cosine $\mathbf{d}\cdot\mathbf{u}_k$ (shown as blue bars in fig. S6). To assess whether a combination of modes would better describe the transition than any given single mode, we also calculated cumulative overlaps as the square root of the sum of squared overlaps (red curves in fig. S6, which revealed no noticeable improvement). These calculations were also carried out using Python with ProDy (*67*).

LBD transitions

Conformational changes within the LBD layer were calculated as transitions between aligned structures from GluA2/3 M1 and either of the apo GluA2 homomer (PDB 4U2P) and an antagonist-bound GluA2 homomer (PDB 3KG2) as described above for the NTD transition. The correlation cosine between these transitions was 0.95, confirming that they follow a shared pathway. The transition between PDB 3KG2 and GluA2/3 M1 was also calculated using the morph command of PyMOL for creation of Movie 2.

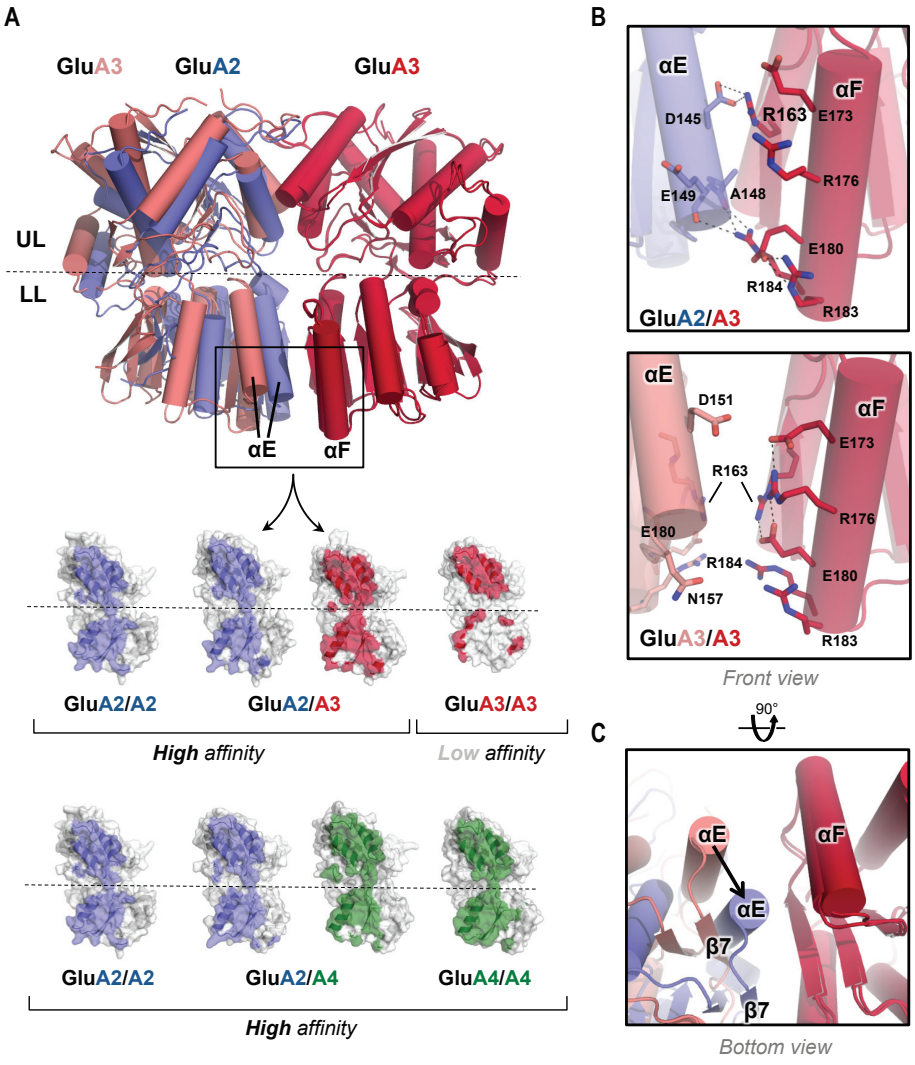

Fig. S1

A comparison between the GluA2/3 heterodimer and a GluA3 homodimer. (A) The GluA3 homodimer (PDB 3O21, dimer CD) is superposed on the GluA2/A3 heterodimer via the GluA3 chain of the heteromer, showing a separation of the lower lobes as compared to the heteromer (top panel). Homo *vs* heteromeric interfaces are compared in an open view of the dimer (lower panel, surface representation). Interface residues are colored blue (GluA2) and red (GluA3), showing the difference in buried surface area between GluA3 homo and heterodimers, which correlates with differences in affinity. The equivalent interface is shown for the GluA2/4 heterodimer below with GluA4 interface residues in green. **(B)** Zooms into the LL dimer interface indicating specific contacts mediating tighter packing in the GluA2/3 heteromer (*top*) that neutralise the charge repulsion seen in the GluA3 homomer (*bottom*). **(C)** A bottom view highlighting the change in position of the partner subunit between the GluA3 homomer and the GluA2/3 heteromer.

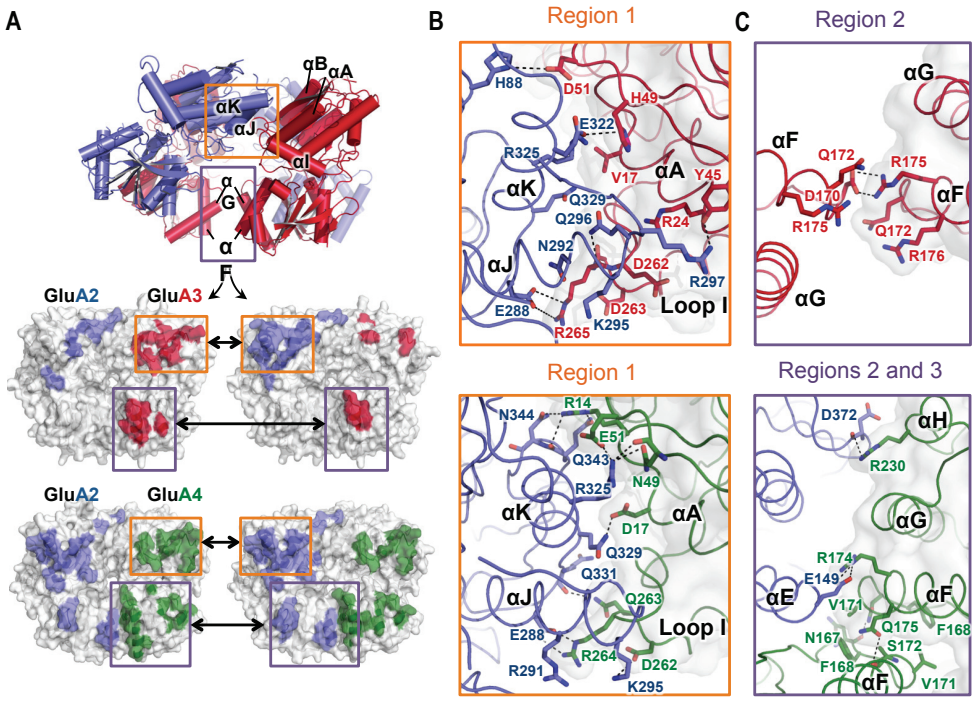

Fig. S2

NTD heterotetramer contacts. (A) Open views are shown for the GluA2/4 (blue/green) and GluA2/3 (blue/red) NTD heterotetramers, highlighting the main contact regions. Lower lobe contacts are tighter in GluA2/4 with the GluA2/3 exhibiting a tilt of ~ 30^{o} (see Fig. S3A). **(B-C)** A zoom-in of the upper lobe tetramer interface (region 1) **(B)** and the lower lobe tetramer interface (regions 2 and 3) **(C)** are shown for the GluA2/3 and GluA2/4 illustrating key polar contacts. In addition to the shared contacts mediated by helix F of the two non-GluA2 chains (region 2), the GluA2/4 interface also includes additional contacts between GluA4 and GluA2 (region 3). Of note, a highly conserved arginine in region 3 (Arg174 in GluA4), which forms a salt-bridge with GluA2 Glu149, also stabilizes the N-shaped tetramer interface in GluA2 homomers.

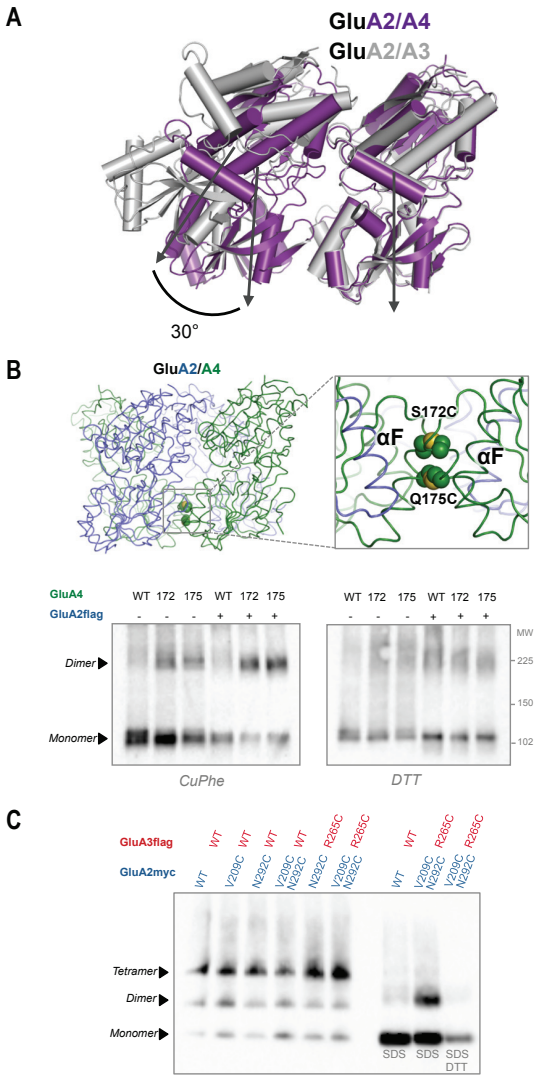

Fig. S3

Comparison of the GluA2/3 and GluA2/4 interdimer arrangements and lower lobe crosslinking. (A) GluA2/3 (grey) and GluA2/4 (purple) tetramers are aligned over a single non-GluA2 subunit to highlight the LL separation between heterodimers in GluA2/3. For each dimer only one subunit is shown. The GluA2/4 NTD lower lobes are closer together, enabling additional contacts in region 2 (between the two non-GluA2 subunits) and further contacts between GluA2 and GluA4 (region 3). The black arrows indicate the symmetry axes of the dimer interfaces and the angle of 30° indicates the difference between GluA2/3 and GluA2/4. **(B)** Cysteine crosslinking of O-shape region 2 in GluA4-containing homomers (lanes 1-3) and heteromers (lanes 4-6) also produces DTT-sensitive dimers. The top panel indicates the crosslinked residues in the structure. **(C)** Native gels confirm that both the N and O shapes form tetrameric contacts within GluA2/3 receptors (lanes 2 to 4) and crosslinking them both does not result in higher order oligomers (lane 5). In the presence of SDS these tetramers are denatured resulting in DTT-sensitive dimers and no higher order oligomers (lanes 7 and 8). Lanes 1 and 6 show a wild-type controls.

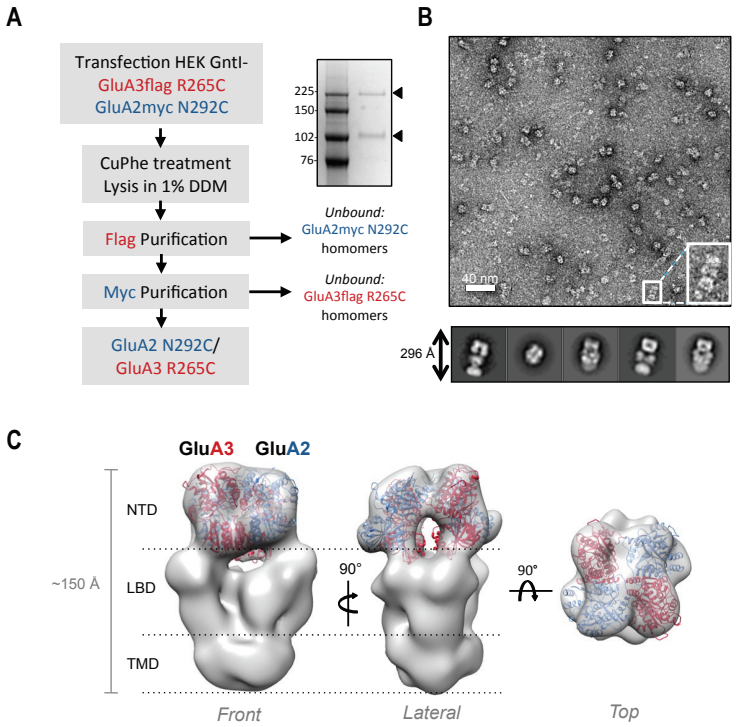

Fig. S4

Negative stain EM of the apo GluA2/3 heteromer. (A) Purification scheme of the GluA2/3 heteromer with a Coomassie-stained SDS gel showing the product. Arrows indicate crosslinked dimers and non-crosslinked monomers. **(B)** Sample image of a uranyl formate stained GluA2/3 crosslinked sample at a nominal magnification of 30,000x and ~1 µm defocus; representative 2D classes are shown below. **(C)** Different views of the 3D reconstruction at ~ 20 Å resolution with the GluA2/3 NTD crystal structure fitted.

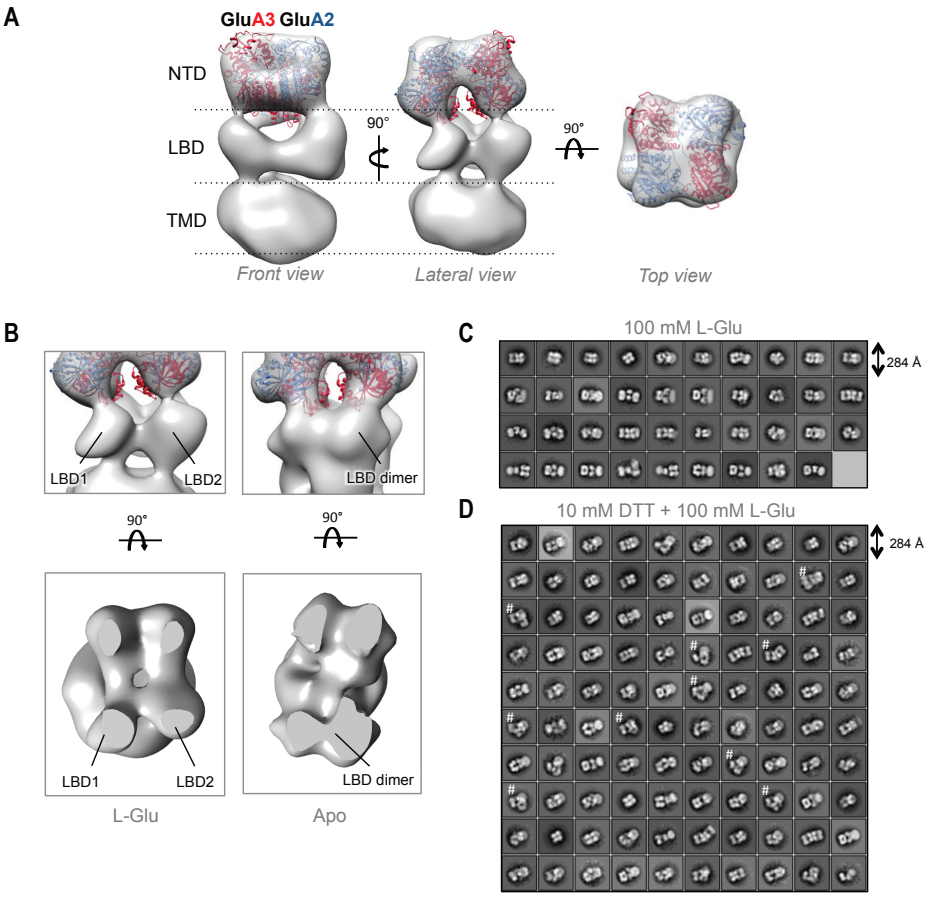

Fig. S5

Negative stain single-particle reconstruction EM of GluA2/3 in the presence of glutamate and glutamate + DDT. (A) Treating crosslinked GluA2/3 heteromers with glutamate resulted in conformational changes within the LBD layer, further supporting the functionality of receptors with NTDs locked in the O shape. Despite the LBD heterogeneity, it was still possible to generate the 3D model shown. **(B)** A zoom-in of the LBD layer (*left*) is compared to that from the ligand free condition (*right*). Agonist binding induces separation of LBDs as previously observed (*21, 22*) and heterogeneity within the layer (indicated by the poor map quality in this region). Below are top views of LBD layers from each model. **(C-D)** 2D classes of glutamate-treated receptors before **(C)** and after treatment with DTT **(D)**. After DTT treatment, there is considerable heterogeneity within the NTD layer, too. In this dataset the NTD was very flexible as indicated by the 2D classes marked with "#". It was not possible to generate a 3D model from this data.

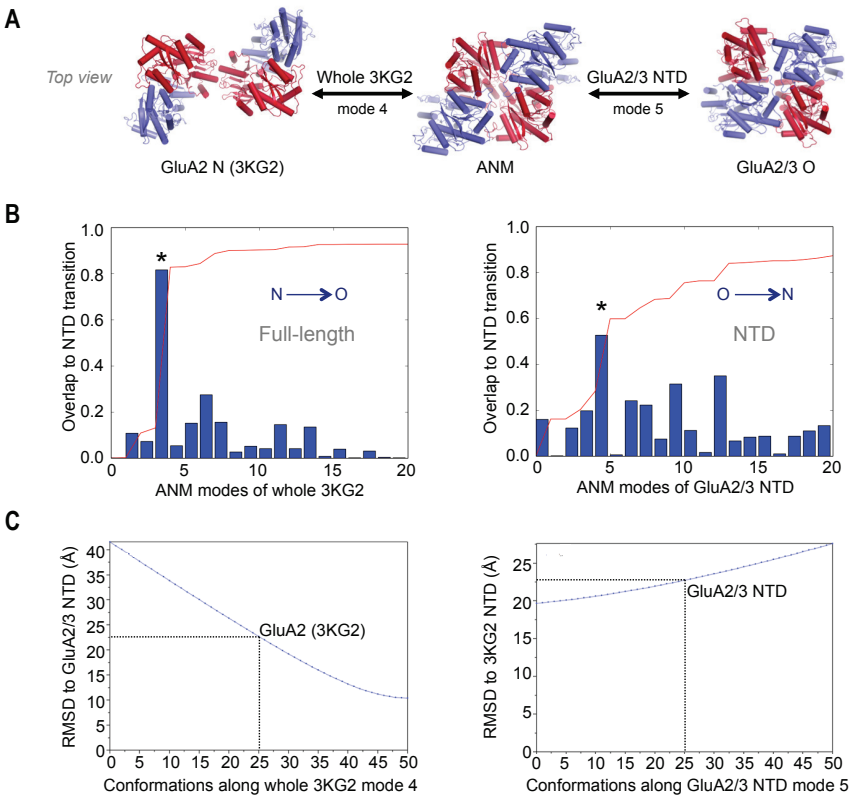

Fig. S6

NTD structural transitions from anisotropic network model (ANM) analysis. (A) The N-shaped NTD arrangement seen in GluA2 homomers (*left*; PDB 3KG2) can rearrange towards the O-shape seen in our heteromers (*right*; our GluA2/3 crystal structure) via an ANM intermediate (*middle*) where lower lobe contacts are similar to those seen in N-shaped NTD tetramers. **(B)** The Cα displacements necessary to convert the N-shaped NTD tetramer to our GluA2/3 NTD crystal structure are compared to the ANM modes generated from each of the two structures. Blue bars show the overlaps (correlation cosines) between this transition and the first 20 ANM modes. The red curve shows the cumulative overlap (square root of the sum of squared overlaps). ANM mode 4 of full-length GluA2 (PDB 3KG2; asterisk in *left* panel; see **Movie 1**) overlaps very well with the structural transition (correlation cosine of ~ 0.8). Mode 5 of the GluA2/3 NTD (asterisk in *bottom* panel) shows a moderate overlap for the reverse transition. This mode features a rearrangement of the lower lobe interface (region 2; see **Movie S1**). **(C)** RMSD graphs compare ANM snapshots from the indicated modes to the target structures. Conformations along 3KG2 mode 4 approach the GluA2/3 NTD crystal structure reaching an RMSD of ~ 10 Å (left panel). By contrast, GluA2/3 mode 5 generates structures that approach the N shape less well (right panel) as expected from the lower overlap. ANM modes are bidirectional harmonic fluctuations about the starting structure, which is conformation 25 and exhibits an RMSD of ~ 23 Å from the target structure.

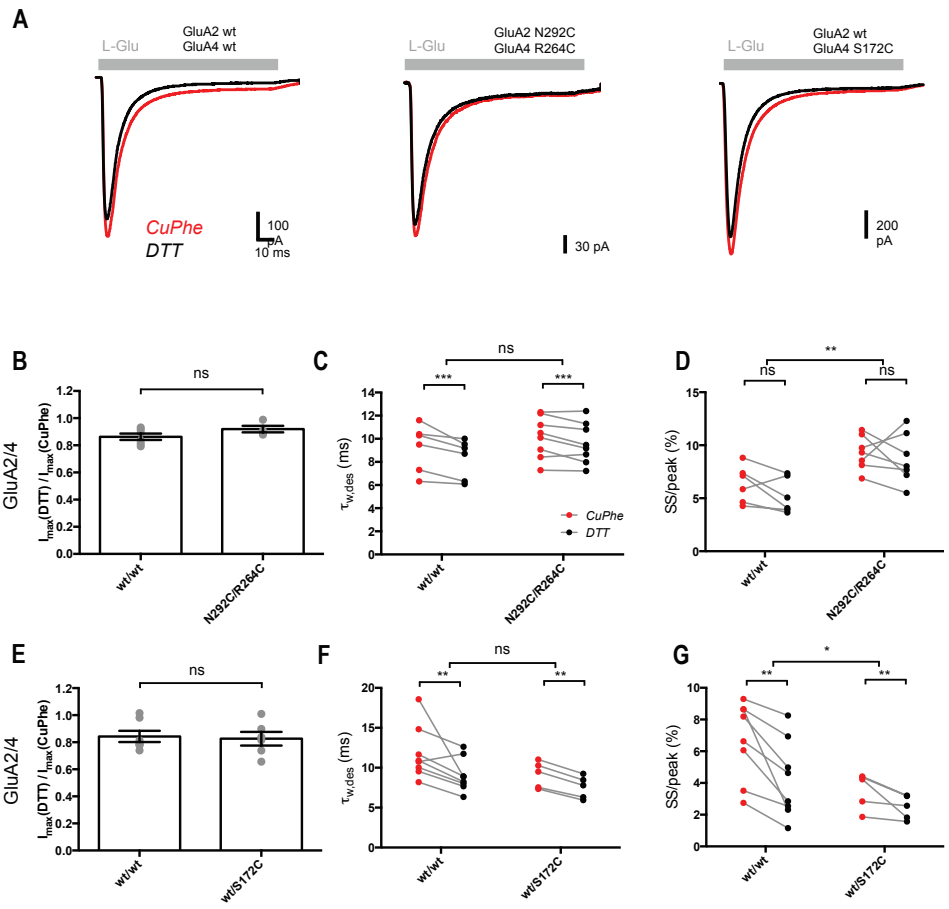

Fig. S7

Electrophysiological characterization of the O-shape-crosslinked GluA2/4 heteromers. (A) Example current traces of HEK293T cells expressing GluA2/4 wt/wt (left), N292C/R264C (middle) or wt/S172C (right) heteromers activated by a 100 ms application of 10 mM glutamate in the presence of 10 µM copper phenanthroline (CuPhe, red) and 10 mM dithiothreitol (DTT, black). **(B)** Summary graph for the effect of the CuPhe/DTT treatment on the amplitude of current responses. For each cell, the ratio of peak currents in both conditions was calculated and plotted. No significant difference between the GluA2/4 wt/wt and the double cysteine mutation pair was found (P = 0.7593; unpaired t-test, *N* = 6 and 8, respectively). Data presented as mean ± SEM. **(C)** Summary graph for the weighted time constant of desensitization ($\tau_{w,des}$; from a two-exponential fit) of GluA2/4 wt/wt or N292C/R264C heteromers, in the presence of CuPhe or DTT. Repeated measures (RM) two-way ANOVA reveals a significant main effect of the CuPhe/DTT treatment (***P = 0.0007) but no effect of the Cys-Cys mutation (P = 0.2731) and no interaction between the two factors (P = 0.2119). *N* = 6 and 8, respectively (also applies to **(D)**). **(D)** As **(C)**, comparing the relative steady state vs. peak currents (SS/Peak). RM two-way ANOVA: significant main effect of the mutation (**P = 0.0033), no effect of the treatment (P = 0.1691), no interaction (P = 0.6381). **(E)** As **(B)**, comparing GluA2/4 wt/wt and wt/S172C heteromers. No significant difference for the peak amplitude ratios (P = 0.7979, *N* = 7 and 6, respectively). **(F)** As **(C)**, $\tau_{w,des}$ for GluA2/4 wt/wt vs. wt/S172C. RM two-way ANOVA: significant main effect of the

treatment (**P = 0.0095), no effect of the mutation (P = 0.1066), no interaction (P = 0.4209). *N* = 7 and 5, respectively (also applies to **(G)**). **(G)** As **(D)**, SS/Peak for GluA2/4 wt/wt vs. wt/S172C. RM two-way ANOVA: significant main effect of the treatment (**P = 0.0015) and of the mutation (*P = 0.0450), no interaction (P = 0.1217).

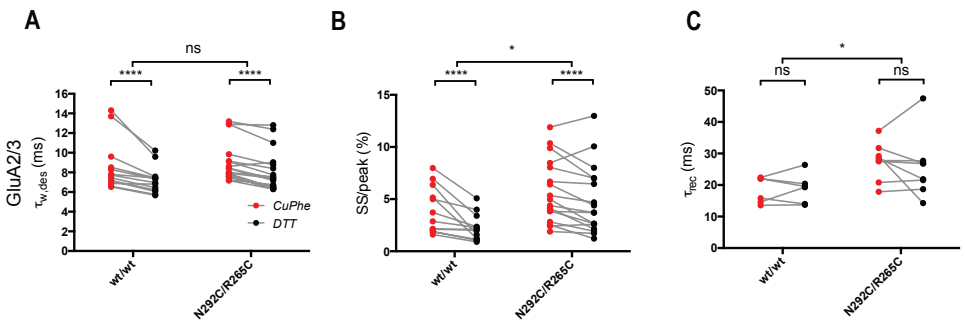

Fig. S8

Electrophysiological characterization of the O-shape-crosslinked GluA2/3 heteromers. (A) Summary graph for the weighted time constant of desensitization ($\tau_{w,des}$; from a two-exponential fit) of GluA2/3 wt/wt or N292C/R265C heteromers, in the presence of CuPhe or DTT (example traces in **Fig. 2E**). Repeated measures (RM) two-way ANOVA shows a significant main effect of the CuPhe/DTT treatment (****P < 0.0001), no effect of the Cys-Cys mutation (P = 0.4014) and no interaction between the two factors (P = 0.1606). *N* = 13 and 18, respectively (also applies to **(B)**). **(B)** As **(A)**, comparing the relative steady state vs. peak currents (SS/Peak). RM two-way ANOVA: significant main effect of the mutation (*P = 0.0336) and of the treatment (****P < 0.0001), no interaction (P = 0.4911). **(C)** As **(A)**, comparing the time constant of recovery from desensitization (τ_{rec}). RM two-way ANOVA: significant main effect of the mutation (*P = 0.0359), no effect of the treatment (P = 0.6655), no interaction (P = 0.4640). *N* = 6 and 8, respectively.

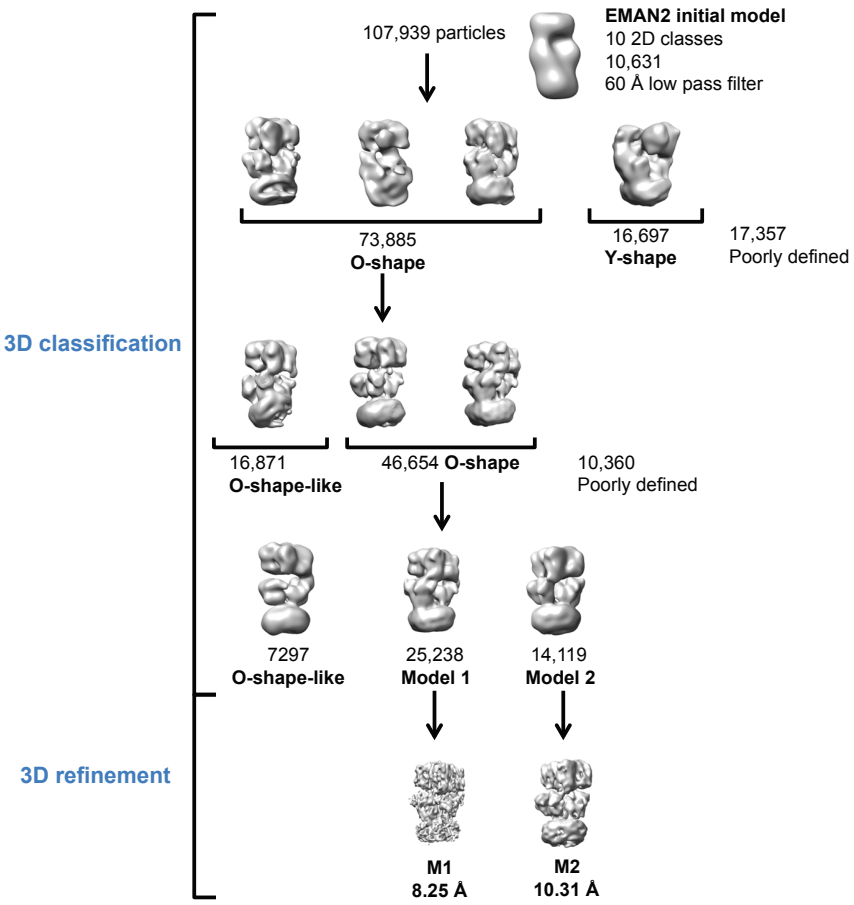

Fig. S9

3D-classification and refinement of the GluA2/3 cryo-EM data. 107,939 particles were classified into five groups using an *ab initio* model generated with EMAN2. While one class featured the classical Y-shape, three other classes had O-like features, and a fifth class eliminated false positives. Two additional steps of classification using a soft mask led to the M1 and M2 models with 25,238 and 14,119 particles, respectively. After refinement, the M1 and M2 models reached resolutions of 8.25 and 10.3 Å, respectively.

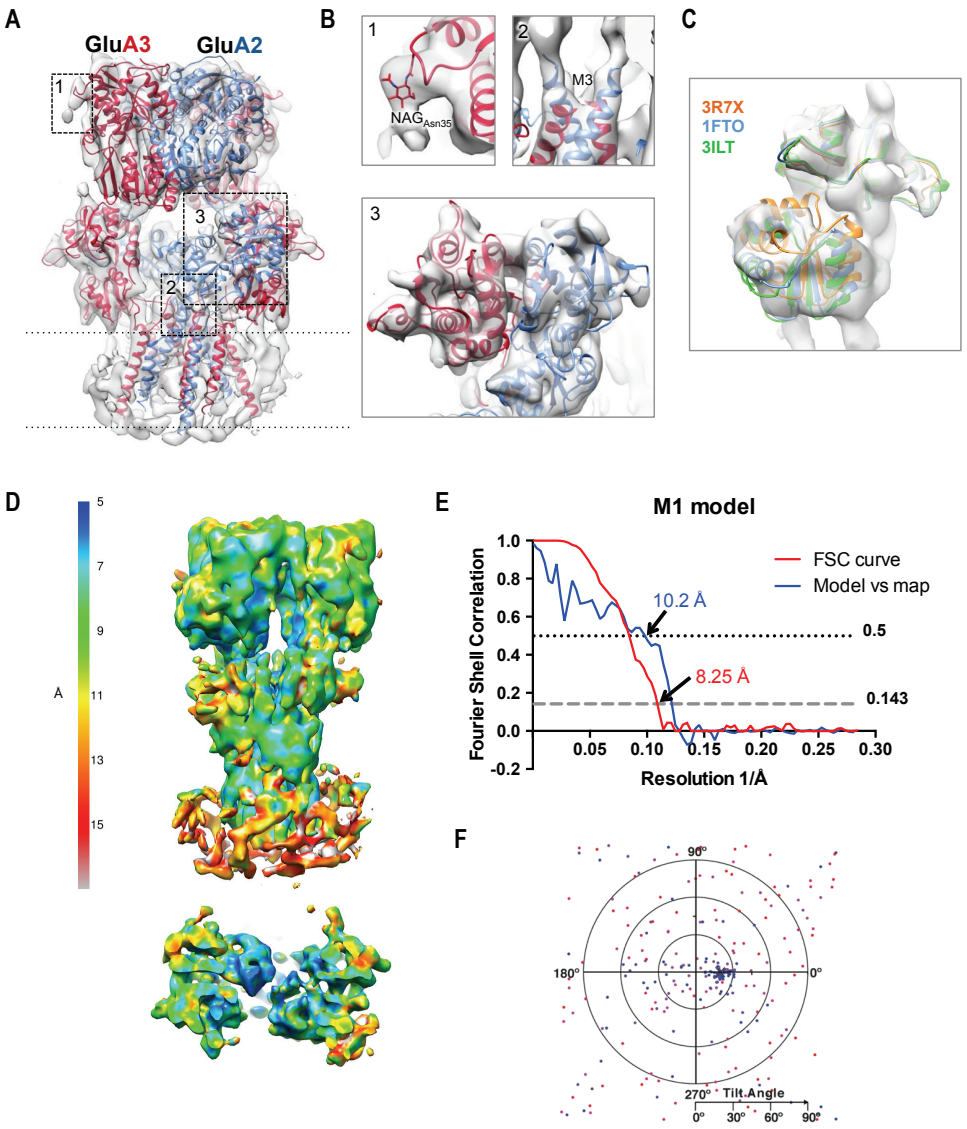

Fig. S10

M1 model fitting and validation. (A) Front view of the M1 model with the nine individual domain crystal structures fitted in the density. **(B)** Closer zooms are shown for the boxed regions in (**A**): **1**. density at the Asn35 sugar, specific to the GluA3 subunits, **2**. the asymmetry seen at the pore opening, and **3.** the good fit at the LBD layer. **(C)** Fits of open and closed LBDs (orange and green) are compared against the LBD chosen by NORMA for GluA2 (blue). The open and closed LBDs clearly fit less well with portions extruding from the density. **(D)** Local map resolution as calculated with ResMap. A side view of the receptor is shown together with the top view of the LBD layer. **(E)** Fourier Shell Correlation for the two independently refined halves of the dataset (gold-standard FSC) for the M1 reconstruction and model are shown. The resolution of M1 map at a correlation of 0.143 is 8.25 Å. The resolution of the model *versus* map at an FSC of 0.5 is 10.2 Å. **(F)** Tilt pair validation using 762 particle pairs acquired at 0 and 20º tilt angle is shown. The position of each dot represents the direction and the amount of tilting for a particle pair in polar coordinates. Blue dots correspond to in-plane tilt transformations;

red and purple dots correspond to out-of-plane tilt transformations. Blue dots cluster at a tilt angle of approximately 20°.

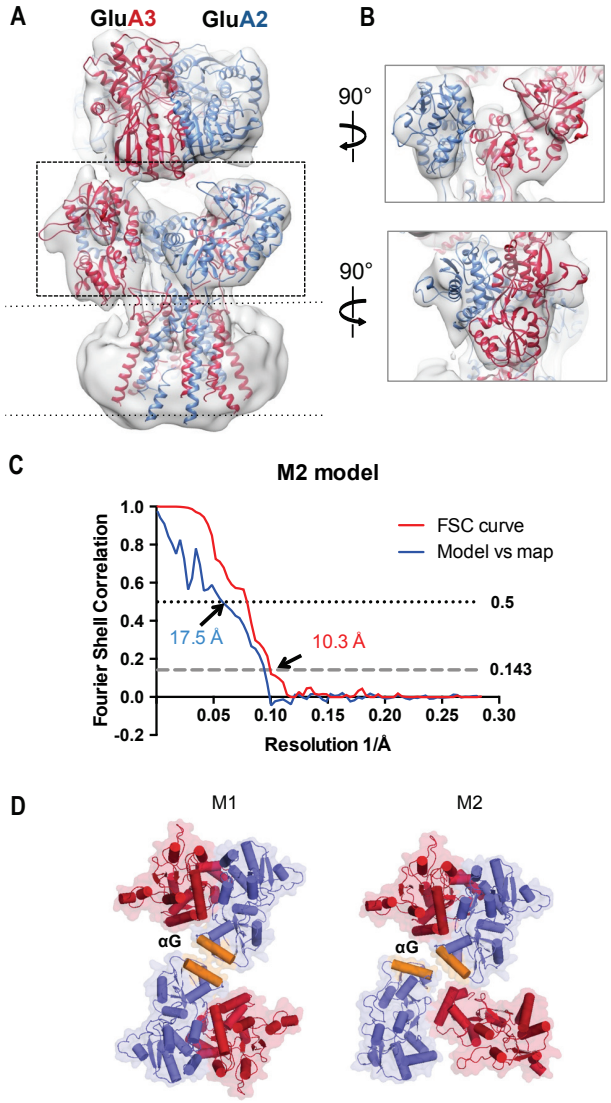

Fig. S11

M2 model fitting and validation. (A) Front view of the M2 model with the nine individual domain crystal structures fitted in the density. **(B)** Side views of the two LBD pairs highlight the separation of the BC pair (*top*) and the dimer formed by the AD pair (*bottom*). **(C)** FSC and model *vs* map correlations showing a resolution of 10.3 Å at the gold-standard of 0.143. Xmipp was used to calculate the model vs map correlation showing a good correlation up to 17.5 Å resolution. For this model a larger difference between the FSC and the model vs map is observed. It is likely that the model suffers from heterogeneity and therefore the high resolution is obscured. Indeed only individual domains and not secondary structures are seen in the map. **(D)** A top view of the LBD layers of M1 and M2 are shown as in **Fig. 6B** for M1. These are rotated to be comparable to **Fig. 4B**.

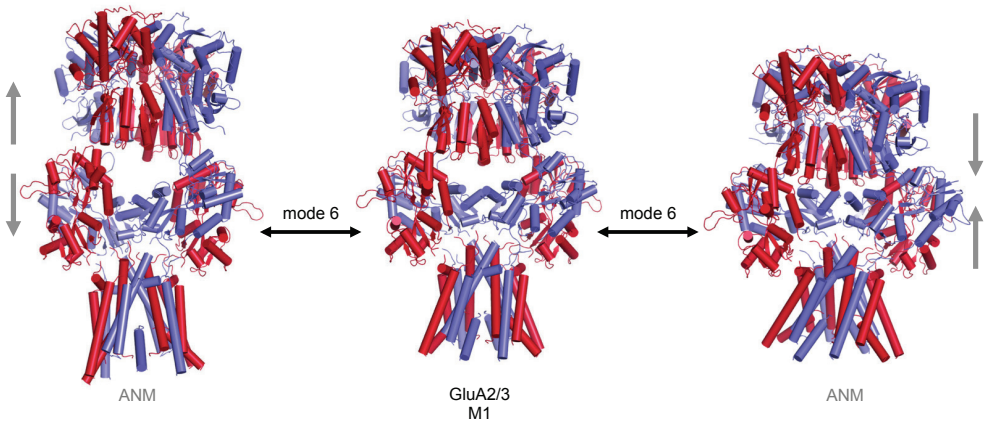

Fig. S12

ANM analysis of GluA2/3 cryo-EM model 1 (M1) reveals that this structure can undergo further vertical compression. Low energy mode 6 enables M1 (*middle*) to be stretched (*left*) and further compressed (*right*). The extent of motion is arbitrary and was chosen to illustrate the direction of motion without introducing substantial clashes.

Table S1.

Crystallographic data collection and refinement statistics

	GluA2/A3 NTD	GluA2/A4 NTD
Data collection		
Source	DLS I04-1	DLS I04-1
Wavelength (Å)	0.920	0.920
Space group	P1	$P2_1$
Cell dimensions		
a, *b*, *c* (Å)	66.27, 78.52, 107.85	61.07, 156.63, 77.12
α, β, γ (°)	94.4, 92.6, 114.9	90, 90.02, 90
Resolution (Å)	41.75 - 2.12	39.16 - 2.50
R_{merge} (%)	10.1 (43.9)	5.6 (35.8)
R_{pim} (%)	10.1 (43.9)	3.7 (23.0)
$CC_{1/2}$	0.99 (0.78)	0.99 (0.95)
$\langle I/\sigma(I) \rangle$	6 (1.9)	12.2 (3.0)
Completeness (%)	90.4 (87.8)	96.3 (96.0)
Redundancy	1.9 (1.9)	3.2 (3.3)
Refinement		
Resolution (Å)	41.75-2.12	39.16 (2.5)
Unique reflections	100,269	45,771
R_{work} / R_{free} (%)	19.2/23.1	17.2/23.8
No. of atoms		
Protein	12011	11156
Ligand/ion	186	62
Water	352	125
Average B-factors (Å^2)		
Protein	39.3	61.2
Ligand/ion	61.4	67
Water	37.7	36.0
R.m.s. deviations		
Bond lengths (Å)	0.016	0.019
Bond angles (°)	1.73	1.62
Ramachandran Plot		
Favoured (%)	1447 (97.8)	1380 (96.2)
Allowed (%)	32 (2.2)	51 (3.6)
Disallowed (%)	0 (0)	3 (0.2)

Table S2.

Cryo EM data collection and model statistics

	M1 class	**M2 class**
Particles	25,238	14,119
Pixel size (Å)	1.76	1.76
Defocus range (μm)	1-4	1-4
Voltage (kV)	300	300
Electron dose (e-/Å^2)	40	40
Resolution (Å)	8.25	10.31

Movie S1.

Top view of ANM mode 5 of the GluA2/3 NTD crystal structure showing a partial O to N transition. The tighter packing of the GluA2/3 NTD heterotetramer acts as a greater barrier to rearrangement, especially under the assumptions of the anisotropic network model. The lower lobe inter-dimer interface (region 2) is most free to rearrange as is seen in a number of the first 5 low energy modes. Mode 5 features a sliding of the two dimers that produces a tighter interface similar to that seen in GluA2 homomers. This creates an intermediate-like that produced by mode 4 of the GluA2 homomer, enabling a complete trajectory in both directions.

Movie S2.

ANM mode 6 of GluA2/3 showing vertical compression and stretching. Compression of the GluA2/3 cryo-EM M1 features a separation of the LBD dimers that accommodates the sinking NTD layer.